J Mater Sci (2009) 44:3833–3840
DOI 10.1007/s10853-009-3519-3

# Structure and electrical properties of $Bi_{0.5}Na_{0.5}TiO_3$–$Bi_{0.5}K_{0.5}TiO_3$–$BiCoO_3$ lead-free piezoelectric ceramics

**Changrong Zhou · Xinyu Liu · Weizhou Li · Changlai Yuan · Guohua Chen**

Received: 4 December 2008 / Accepted: 25 April 2009 / Published online: 15 May 2009


**Abstract** Lead-free piezoelectric ceramics $(1 - x - y)Bi_{0.5}Na_{0.5}TiO_3$–$xBi_{0.5}K_{0.5}TiO_3$–$yBiCoO_3$ ($x = 0.12$–$0.24$, $y = 0$–$0.04$) have been fabricated by a conventional solid-state reaction method, and their structure and electrical properties have been investigated. The XRD analysis shows that samples with $y \leq 0.03$ exhibit a pure perovskite phase and very weak impurity reflections can be detected in the sample with $y = 0.04$. With $x$ increasing from 0.12 to 0.24 and $y$ increasing from 0 to 0.04, the ceramics transform gradually from a rhombohedral phase to a tetragonal phase and rhombohedral–tetragonal phase coexistence to a pseudocubic phase, respectively. The morphotropic phase boundary (MPB) of the system between rhombohedral and tetragonal locates in the range of $x = 0.18$–$0.21$, $y = 0$–$0.03$. The ceramics near the composition of the MPB have good performances with piezoelectric constant $d_{33} = 156$ pC/N and electromechanical coupling factor $k_p = 0.34$ at $x = 0.21$ and $y = 0.01$, which attains a maximum value in this ternary system. Adding content of $BiCoO_3$ leads to a disappearance of the response in the curves of dielectric constant-temperature to the ferroelectric–antiferroelectric transition. The temperature dependence of dielectric properties suggests that the ceramics are relaxor ferroelectrics. The results show that $(1 - x - y)Bi_{0.5}Na_{0.5}TiO_3$–$xBi_{0.5}K_{0.5}TiO_3$–$yBiCoO_3$ ceramics are good candidate for use as lead-free ceramics.

C. Zhou (✉) · X. Liu · C. Yuan · G. Chen
Guangxi Key Laboratory of Information Materials, Guilin University of Electronic Technology, Guilin, Guangxi 541004, People's Republic of China
e-mail: zcr750320@yahoo.com.cn

W. Li
School of Materials Science and Engineering, Guangxi University, Nanning, Guangxi 530004, People's Republic of China

## Introduction

Currently, piezoelectric ceramics based on lead zirconate titanate (abbreviated as PZT) system dominate piezoelectric ceramic application for their excellent piezoelectric properties. However, the evaporation of toxic lead during the fabrication of the ceramics will cause environmental problems which are also related to the use and disposal of components. Thus, there is an increasing interest in developing lead-free piezoelectric ceramics to replace PZT-based piezoelectric ceramics [1].

Among the lead-free piezoelectric materials [2–5], one of the most studied compounds is ferroelectric bismuth sodium titanate $(Bi_{0.5}Na_{0.5})TiO_3$ (BNT), which was discovered by Smolenskii and Aganovskaya and is one of the most important lead-free piezoelectric materials with a perovskite crystal structure [6]. It has interesting electrical properties (good dielectric constant ($\varepsilon_r$) and acceptable piezoelectric coefficient ($d_{33}$)). However, BNT has the drawback of having a high coercive field and a high conductivity, which cause difficulties in the poling process. To improve the piezoelectric properties of BNT ceramics, some investigations have concentrated on the search for a new morphotropic phase boundary (MPB) in the BNT-based binary and ternary systems. It is well known that the MPB plays a very important role in PZT ceramics because the piezoelectric and dielectric properties show a maximum over a specific compositional range around the MPB [7]. Among BNT-based solid states [8–12], the BNT–BKT system has rhombohedra-tetragonal MPB in the range of

0.16–0.20 mol BKT and reveals relatively high piezoelectric and ferroelectric properties at the composition near the MPB [13]. It has been known that multicomponent ceramics usually possess better piezoelectric properties than single or binary-component ceramics [14, 15], and hence R&D effort has always been put on developing new multicomponent piezoelectric ceramics. Meanwhile, perovskite type Bi-based ferroelectrics of $BiMeO_3$ (Me = Fe, Al, Co) have strong ferroelectricity and high Curie temperature [16–18]. Especially, the giant electric polarization more than 150 $\mu C/cm^2$ is predicted for Bi $CoO_3$ on the basis of the first-principles Berry-phase method [18]. Following these, a new ternary BNT-based lead-free ceramic, $(1 - x - y)Bi_{0.5}Na_{0.5}TiO_3$–$xBi_{0.5}K_{0.5}TiO_3$–$yBiCoO_3$ has been developed in our group. However, little is known about the microstructure and electrical of the ceramics. In this study, $(1 - x - y)Bi_{0.5}Na_{0.5}TiO_3$–$xBi_{0.5}K_{0.5}TiO_3$–$yBiCoO_3$ ceramics were prepared by a conventional solid-state sintering processing, and their microstructure, MPB and electrical properties were studied systematically.

## Experimental

A conventional mixed oxide route was utilized to prepare $(1 - x - y)Bi_{0.5}Na_{0.5}TiO_3$–$xBi_{0.5}K_{0.5}TiO_3$–$yBiCoO_3$ (BNT–BKT–BC–$x/y$) ceramics. Reagent grade oxide or carbonate powders of $Bi_2O_3$, $TiO_2$, $Co_2O_3$, $K_2CO_3$, and $Na_2CO_3$ were used as starting materials. The powders were ball-milled for 12 h and calcined at 800–900 °C for 2 h. After calcination, the mixture was ball-milled for 24 h, dried and

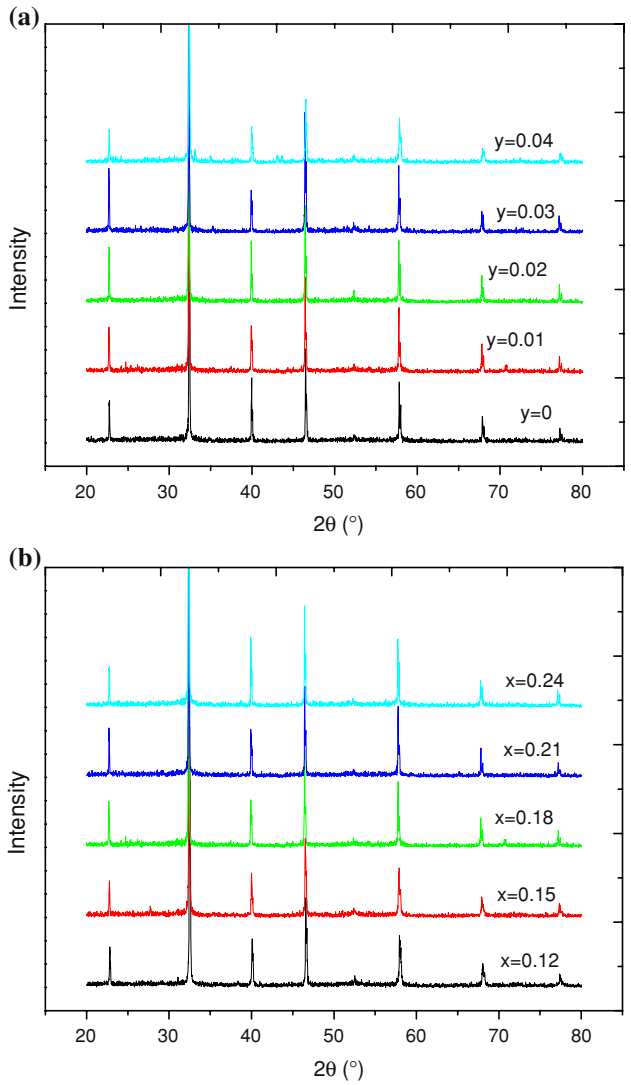


**Fig. 1** XRD pattern of BNT–BKT–BC–$x/y$ ceramics: **a** $x = 0.18$; **b** $y = 0.01$

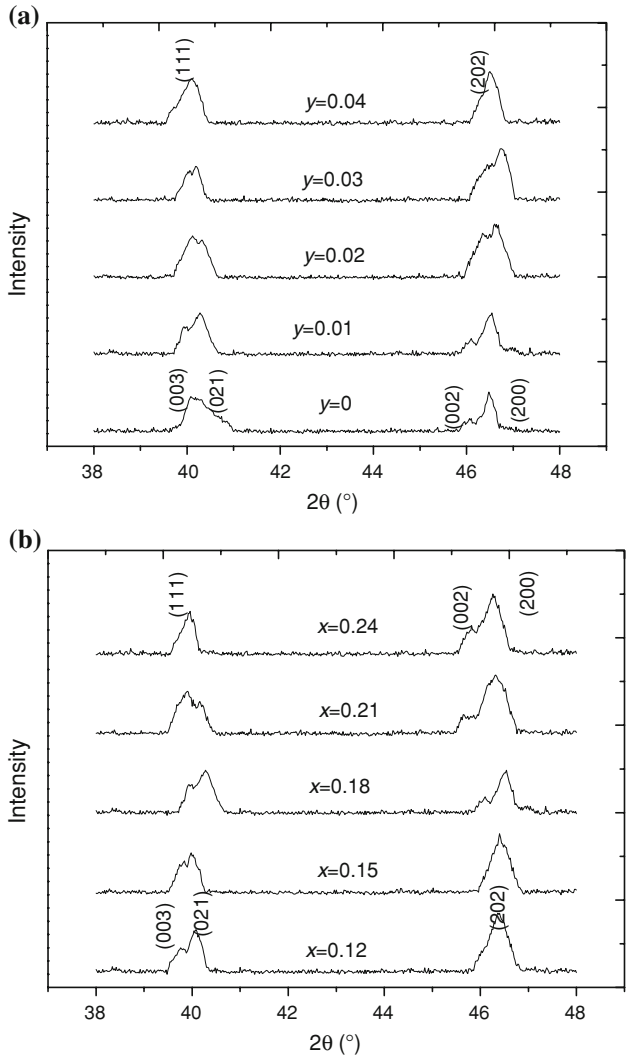


**Fig. 2** XRD pattern of BNT–BKT–BC–$x/y$ ceramics in the $2\theta$ range of 38–48°: **a** $x = 0.18$; **b** $y = 0.01$

granulated with PVA as a binder. The granulated powders were pressed into discs with diameter 18 mm and thickness 1.2 mm. The compacted discs were sintered at 1130–1160 °C for 2 h in air. Silver paste was fired on both faces of the discs at 650 °C as electrodes. The specimens for measurement of piezoelectric properties were poled in a silicon oil at 40–50 °C under 3–4 kV/mm for 15 min.

The crystalline phase of sintered ceramics was identified by the X-ray diffractometer (Bruker D8-Advance) with Cu $K\alpha$ radiation ($\lambda = 1.5418$ Å) and graphite monochrometer. The microstructure of sintered samples was observed by a scanning electron microscope (JSM–5610LV). Piezoelectric properties were measured using an impedance analyzer (Agilent 4294A) by a resonant and anti-resonant method. Piezoelectric constant $d_{33}$ was measured by means of a quasi-static $d_{33}$ meter (ZJ–3A, China) based on the Berlincourt method at 110 Hz. The dielectric properties were investigated using an impedance analyzer (Agilent 4294A).

## Result and discussion

The XRD diffraction patterns of BNT–BKT–BC–$x/y$ compositions are shown in Fig. 1. The ceramics with $y \leq 0.03$ possess a pure perovskite structure and very weak impurity reflections can also be detected in the sample with $y = 0.04$. Figure 2 shows the XRD diffraction patterns in the $2\theta$ range of 38–48° for the ceramic specimens with various amounts of BKT and $BiCoO_3$. Obvious splitting of XRD peaks was detected for the specimens with $x = 0.18$–$0.21$ and $y = 0$–$0.03$. They can be assigned to a (003)/(021) peak splitting and a (002)/(200) peak splitting according to a rhombohedral symmetry and a tetragonal symmetry, respectively. This characterizes a coexistence of rhombohedral and tetragonal phases, which is consistent with the nature of the specimen with a MPB composition. The specimens with $BiCoO_3$ content $y \leq 0.03$ ($x = 0.18$) maintained the coexistence of the two phases. Moreover,

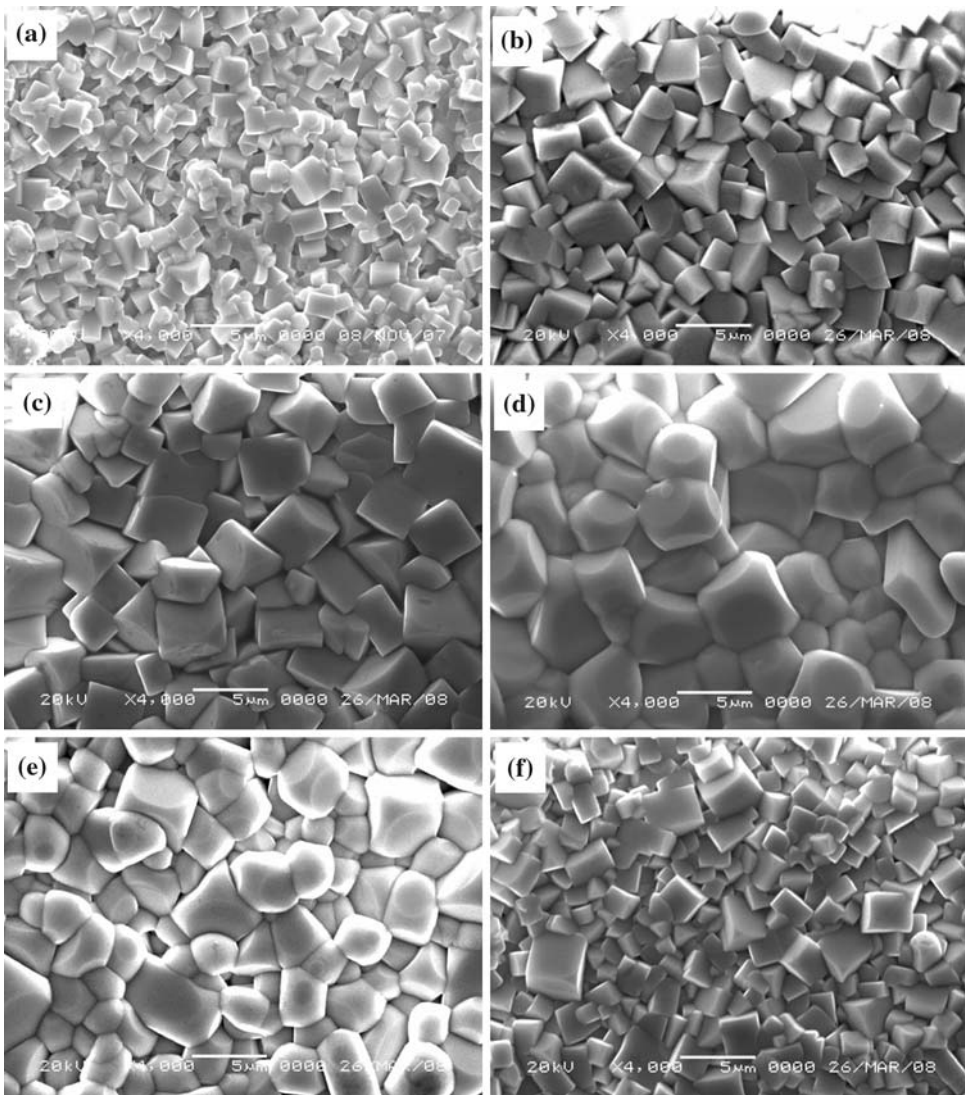


**Fig. 3** SEM images of BNT–BKT–BC–$x/y$ ceramics: **a** $x/y = 0.18/0$; **b** $x/y = 0.18/0.02$; **c** $x/y = 0.18/0.04$; **d** $x/y = 0.12/0.01$; **e** $x/y = 0.21/0.01$, and **f** $x/y = 0.24/0.01$

the (002)/(200) peak splitting is obvious and (003)/(021) peak merges into single (111) peak when $x = 0.24$, which indicates that the crystalline structure varies from the coexistence of rhombohedral and tetragonal phases to tetragonal phase. On the other hand, (003)/(021) peak and (002)/(200) peak merge into single (111) peak and (202) peak when $y = 0.04$, which indicates that the crystalline structure turns into pseudocubic phase. It can be concluded from the above results that the composition range of MPB lies in $x = 0.18$–$0.21$ and $y = 0$–$0.03$ for BNT–BKT–BC–$x$/$y$ ceramics.

The SEM micrographs of the BNT–BKT–BC–$x$/$y$ ceramics are shown in Fig. 3. All the ceramics can be well-sintered at 1130–1160 °C for 2 h, and are dense and pore-free. For the BNT-BKT-BC–$x$/0.01 ceramics, the grains become evidently smaller with the concentration $x$ of BKT increasing from 0.18 to 0.24. It can be attributed to that $K^+$ concentrates near grain boundaries and decreases their mobility substantially as densification occurs. The reduction in the mobility of the grain boundary weakens the mass transport. As a result, grain growth is obviously inhibited and smaller grains are formed in the BNT–BKT–BC–$x$/0.01 ceramics at high concentration $x$ of BKT. On the other hand, the grain size increases as the content $y$ of BC increases. According to Shannon's effective ionic radii with a co-ordination number of six, $Co^{3+}$ has a radius of 0.61 Å, which equal that of $Ti^{4+}$(0.61 Å) [19]. Therefore, $Co^{3+}$ can enter into the sixfold coordinated B site of the perovskite structure to substitute for $Ti^{4+}$ because of radius matching. Due to a lower valence state compared with $Ti^{4+}$, the incorporation of $Co^{3+}$ into the octahedral site of the structure produced excess negative charges. To maintain an overall electrical neutrality, oxygen vacancies were created for compensation purposes. As is generally recognized, the presence of oxygen vacancies in oxide systems is beneficial to mass transport during sintering. This is assumed to be responsible for the promoted grain growth as the content $y$ of BC increases. Moreover, the introduction of Bi significantly decreases the sintering temperature of BNT–BKT–BC–$x$/$y$ ceramics, and thus greatly promotes the grain growth because of the formation of liquid phase due to the low melting point of Bi-containing compounds.

Figure 4 reveals the dielectric constant $\varepsilon_r$ and dielectric loss tan $\delta$ for the unpoled samples as a function of BKT and BC content at room temperature, respectively. With the increase of BC amount, the $\varepsilon_r$ and tan $\delta$ of BNT–BKT–BC–0.18/$y$ ceramics displayed a monotonic decline. Unlike BNT–BKT–BC–0.18/$y$ ceramics, the $\varepsilon_r$ and tan $\delta$ of BNT–BKT–BC–$x$/0.01 ceramics exhibits an obvious increase with increasing content $x$ of BKT. The monotonic decrease of the $\varepsilon_r$ and tan $\delta$ of BNT–BKT–BC–0.18/$y$ ceramics can be attributed to the clamping effect associated with oxygen vacancies [14]. The clamping effect hindered reorientation

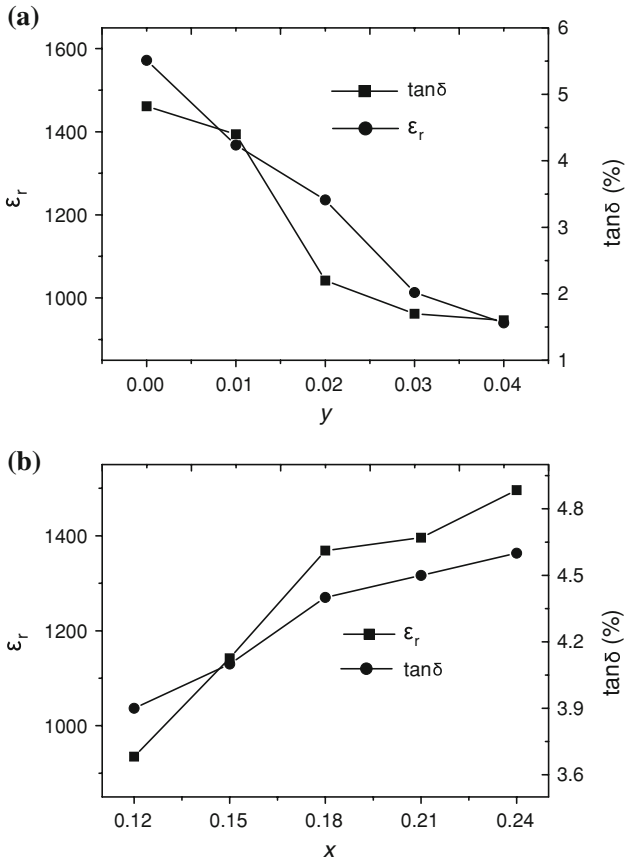


**Fig. 4** Variations of dielectric constant $\varepsilon_r$ and dielectric loss tan $\delta$ of the BNT–BKT–BC–$x$/$y$ ceramics: **a** $x = 0.18$; **b** $y = 0.01$

of dipoles or ferroelectric domains which is considered to be responsible for the decrease of dielectric constant and dielectric loss. Moreover, the radius of $K^+$ is 1.64 Å, which is close to that of $Na^+$(1.39 Å). Therefore, $K^+$ can enter into A site of the perovskite structure to substitute for $Na^+$. The substitution of the relatively larger $K^+$ for the relatively smaller $Na^+$ led to an enlargement of the unit cells. That promoted the reorientation of dipoles or ferroelectric domains which is considered to be responsible for the increase of dielectric constant and dielectric loss for BNT–BKT–BC–$x$/0.01 ceramics.

Figure 5 shows the variation of piezoelectric constant $d_{33}$ and the planar electromechanical coupling factor $k_p$ for BNT–BKT–BC–$x$/$y$ ceramics. For all the ceramics, the $d_{33}$ and $k_p$ increase obviously with increasing $x$ and $y$ and then decrease, reaching maximum values of $d_{33} = 156$ pC/N and $k_p = 0.34$ at $x = 0.21$ and $y = 0.01$. Figure 6 presents the mechanical quality factor $Q_m$ of BNT–BKT–BC–$x$/$y$ ceramics as a function of BKT and BC content. It can be seen that $Q_m$ of BNT–BKT–BC–0.18/$y$ ceramics keeps increasing with increasing $y$, and $Q_m$ of BNT–BKT–BC–$x$/0.01 ceramics decreases sharply with increasing $x$ and then increases with $x$ further increases. The variation of $Q_m$

for BNT–BKT–BC–0.18/$y$ ceramics and BNT–BKT–BC–$x$/0.01 ceramics may be attributed to the grain size effect and MPB effect, respectively.

Bismuth lies next to lead in the periodic table and its atomic weight is as large as that of lead. Moreover, the electronic configuration of $Bi^{3+}$ is identical to that of $Pb^{2+}$. Therefore, it is assumed that the large ferroelectricity of BNT-based solid solutions is attributed to $(Bi_{0.5}Na_{0.5})^{2+}$ ions, especially $Bi^{3+}$ ions, in the A-site of $ABO_3$ perovskite structure [20, 21]. On the other hand, the clamping effect caused by oxygen vacancies can restrain the motion of ferroelectric domains, and thus reduce the piezoelectric properties. The variation of $d_{33}$ and $k_p$ for BNT–BKT–BC–0.18/$y$ ceramics can be roughly understood in relation to the co-contribution of the bismuth content effect and the oxygen vacancy effect. From Fig. 5, one can suggest that the bismuth content seems to be the main contributing factor at relatively low BC amounts, while the oxygen vacancy effect appears to be dominant at relative high BC amounts. The severe degradation in piezoelectricity at higher concentration $y$ of BC (e.g., $y = 0.04$) also can be attributed to the crystal structure converted to pseudocubic phase. The large enhancement in piezoelectric properties of the BNT–BKT–BC–$x$/0.01 ceramics can be attributed to the existence of the MPB because the number of possible spontaneous polarization directions increases at the MPB.

The temperature dependences of the dielectric constant $\varepsilon_r$ and dielectric loss tan $\delta$ for the poled BNT–BKT–BC–$x/y$ samples at 100 Hz, 1, 10, and 100 kHz are shown in Fig. 7. The ceramics exhibit two dielectric anomalies at $T_d$ and $T_m$. $T_d$ is the depolarization temperature which corresponds to the transition from a ferroelectric state to so-called "anti-ferroelectric" state, while $T_m$ is the maximum temperature at which $\varepsilon_r$ reaches a maximum value and corresponds to a transition from an "anti-ferroelectric" state to a paraelectric state [22]. All samples exhibit a strong frequency dependence and a broad peak with diffuse phase transition characteristics, implying that the ceramics are relaxor ferroelectrics. It was also found from Fig. 7 that the low-temperature hump in dielectric constant curve of

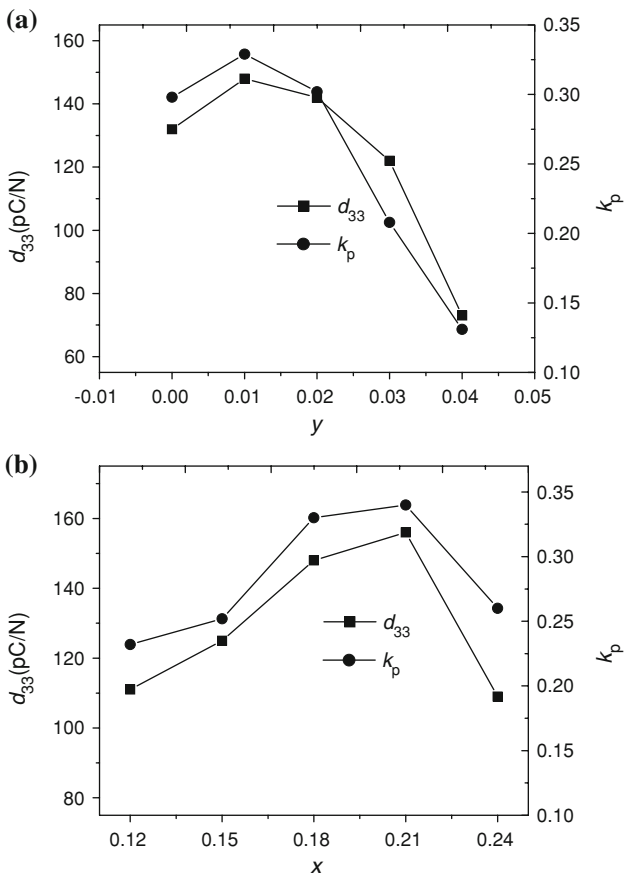


**Fig. 5** Piezoelectric constant $d_{33}$ and planar electromechanical coupling factor $k_p$ of the BNT–BKT–BC–$x/y$ ceramics: **a** $x = 0.18$; **b** $y = 0.01$

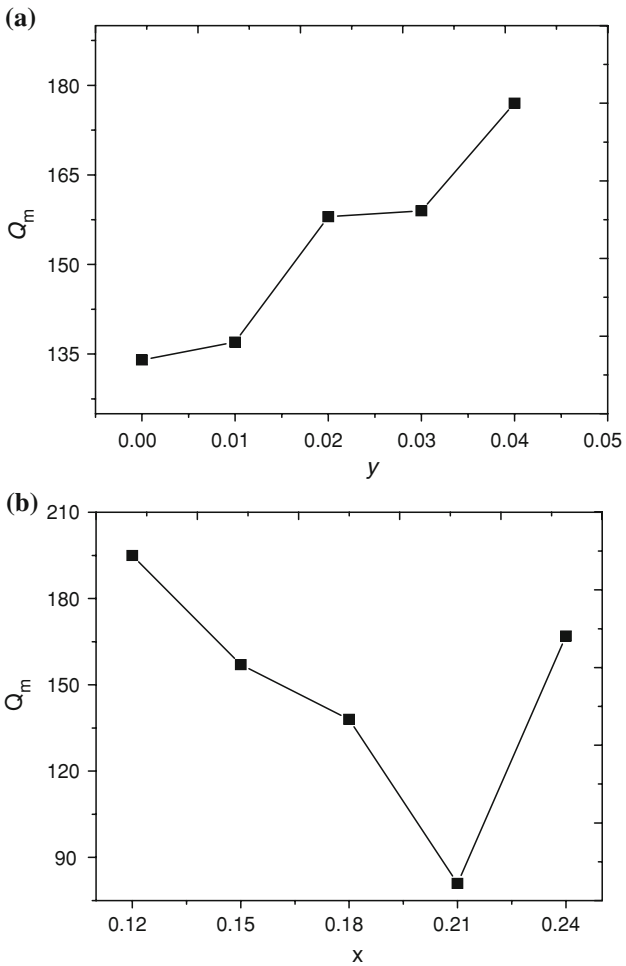


**Fig. 6** Mechanical quality factor $Q_m$ of the BNT–BKT–BC–$x/y$ ceramics: **a** $x = 0.18$; **b** $y = 0.01$

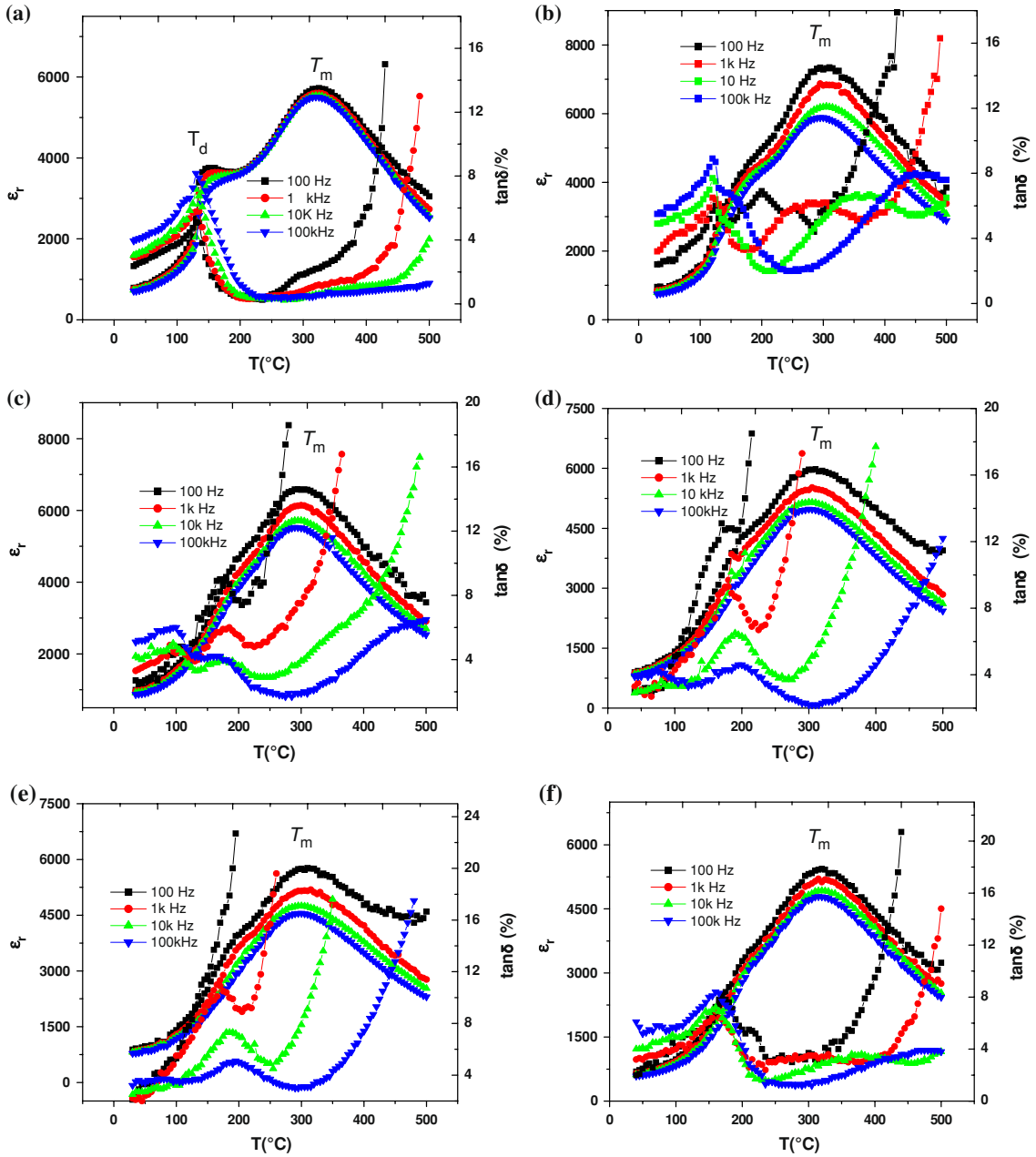


**Fig. 7** Temperature dependences of $\varepsilon_r$ and tan $\delta$ for the poled BNT–BKT–BC–$x/y$ samples: **a** $x/y = 0.18/0$; **b** $x/y = 0.18/0.01$; **c** $x/y = 0.18/0.02$; **d** $x/y = 0.18/0.03$; **e** $x/y = 0.18/0.04$; **f** $x/y = 0.12/0.01$; **g** $x/y = 0.15/0.01$; **h** $x/y = 0.21/0.01$, and **i** $x/y = 0.24/0.01$

BNT–BKT–BC–0.18/$y$ ceramics disappeared slowly with increasing $y$ and it appeared again with increasing $x$ in BNT–BKT–BC–$x$/0.01 ceramics. A similar phenomenon was observed in $(Na_{0.5}Bi_{0.5})_{0.94}Ba_{0.06}TiO_3$ ceramics with a small amount of $Co_2O_3$ added and $(Na_{0.5}Bi_{0.5})_{0.93}Ba_{0.07}TiO_3$ ceramics with a small amount of CoO added [14, 23]. This can be explained in terms of the incorporation of Co into the lattice and generation of oxygen vacancies. Successive ferroelectric–antiferroelectric–paraelectric transition with increasing temperature had previously been observed in varieties of lead-based complex perovskite compounds and BNT-based compositions [24, 25]. The intermediate antiferroelectric state has been strictly be classified as a normal antiferroelectric state and can be explained in light of a subtle modulation of spontaneous polarization [24, 26, 27]. The weak hump in the dielectric constant curve can be regarded as a response to such incommensurate modulation. Based upon the transmission electron microscopy (TEM) observation, it has been revealed that there is a direct interaction between ferroelectric domains and the incommensurate modulation, with ferroelectric domain walls playing a role as barriers [26].

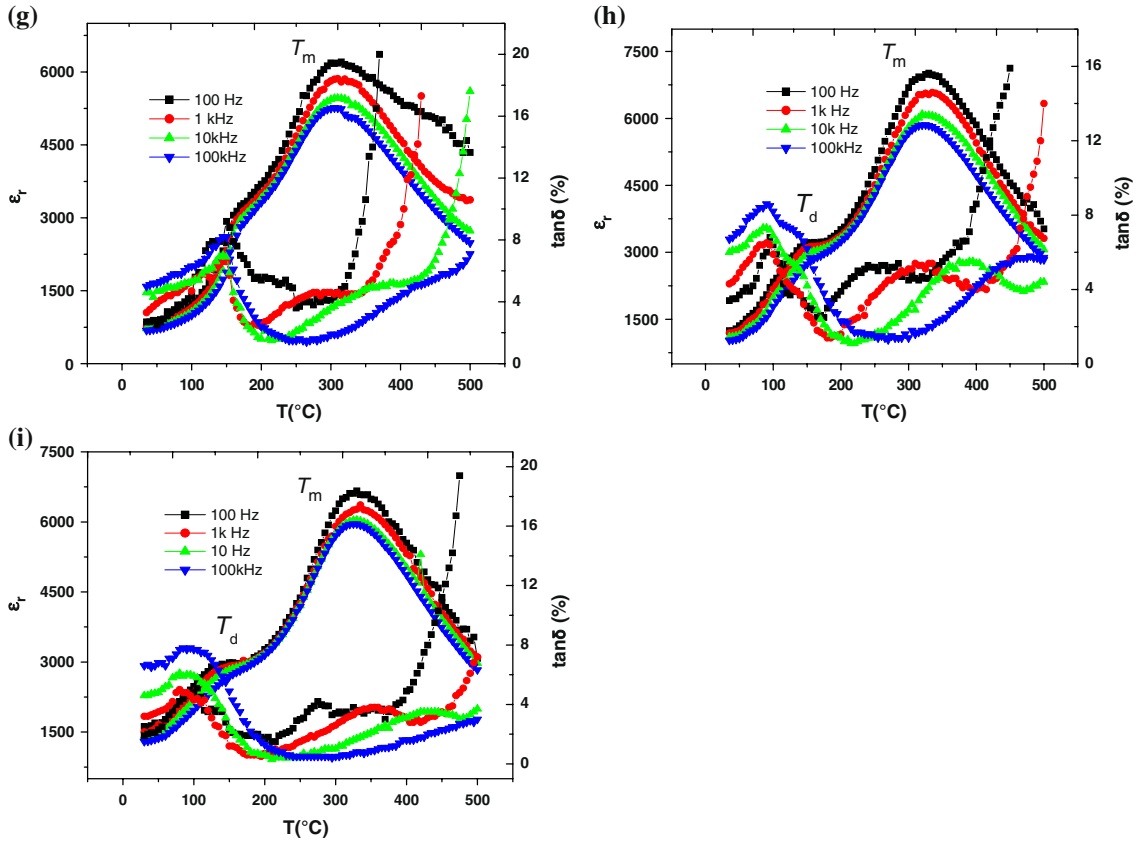


**Fig. 7** continued

As is well known, oxygen vacancies in perovskite-type ferroelectrics have a clamping effect on the motion of domain walls. Then, it is plausible that the clamping effect associated with the appearance of oxygen vacancies caused by adding BC could dynamically suppress the degree of modulating spontaneous polarization. This is believed to be the main reason for the disappearance of the weak hump in the dielectric constant curves of the BNT–BKT–BC–0.18/$y$ ceramics.

## Conclusions

Lead-free piezoelectric ceramics $(1 - x - y)Bi_{0.5}Na_{0.5}TiO_3$–$xBi_{0.5}K_{0.5}TiO_3$–$yBiCoO_3$, a new member of the BNT-based group, has been successfully synthesized by a conventional ceramics technique. The XRD results reveal that a MPB with rhombohedral and tetragonal co-existence for the ceramics lies in the range of $x = 0.18$–$0.21$ and $y = 0$–$0.03$. The piezoelectric properties of the ceramics increase obviously with increasing content of BKT and $BiCoO_3$ and then decrease, reaching maximum values of $d_{33} = 156$ pC/N and $k_p = 0.34$ at $x = 0.21$ and $y = 0.01$. The temperature dependences of dielectric properties show that low-temperature hump in dielectric constant curve disappears slowly with increasing $y$ and appears again with increasing $x$ and the ceramics are relaxor ferroelectrics.

## References

1. Jarupoom P, Pengpat K, Pisitpipathsin N, Eitssayeam S, Inatha U, Rujijanagul G, Tunkasiri T (2008) Curr Appl Phys 8:253
2. Saito Y, Takao H, Tani T, Nonoyama T, Takatori K, Homma T, Nagaya T, Nakamura M (2004) Nature 432:84
3. Suzuki M, Nagata H, Ohara J (2003) Jpn J Appl Phys 42:6090
4. Sawada T, Ando A, Sakabe Y, Damjanovic D (2003) Jpn J Appl Phys 42:6094
5. Zhou CR, Liu XY (2008) Mater Chem Phys 108:413
6. Smolenski GA, Aganovskaya AI (1960) Sov Phys Solid State 1:1429
7. Jaffe B (1971) Piezoelectric ceramics. Academic Press, London, pp 135–170
8. Dai YJ, Pan JS, Zhang XW (2007) Key Eng Mater 336–338:206
9. Yang ZP, Liu B, Wei LL, Hou YT (2008) Mater Res Bull 43:81
10. Takenaka T, Okuda T, Takegahara K (1997) Ferroelectrics 196:175
11. Wang XX, Chan HLW, Choy CL (2003) J Am Ceram Soc 86:1809
12. Nagata H, Koizumi N, Takenaka T (1999) Key Eng Mater 169–170:37
13. Zhao W, Zhou HP, Yan YK, Liu D (2008) Key Eng Mater 368–372:1908

14. Xu Q, Chen M, Chen W, Liu HX, Kim BH, Ahn BK (2008) Acta Mater 56:642
15. Wang XX, Tang XG, Chan HLW (2004) Appl Phys Lett 85:91–94
16. Baettig P, Schelle CF, Lesar R, Waghmare UV, Spaldin NA (2005) Chem Mater 17:1376
17. Woodward DI, Reaney IM, Eitel RE, Randall CA (2003) J Appl Phys 94:3313
18. Uratani Y, Shishidou T, Ishii F, Oguchi T (2005) Jpn J Appl Phys 44:7130
19. Shannon RD (1976) Acta Crystallogr A 32:751
20. Nagata H, Takenaka T (1997) Jpn J Appl Phys 36:6055
21. Nagata H, Takenaka T (1998) Jpn J Appl Phys 37:5311
22. Lin DM, Kwok KW, Chan HLW (2008) Solid State Ionics 178:1930
23. Li HD, Feng DC, Yao WL (2004) Mater Lett 58:1194
24. Lee JK, Yi JY, Hong KS (2004) J Appl Phys 96:1174
25. Yasuda N, Konda J (1993) Appl Phys Lett 62:535
26. Randall CA, Markgraf SA, Bhalla AS, Baba-Kishi K (1989) Phys Rev B 40:413
27. Randall CA, Bhalla AS (1990) Jpn J Appl Phys 29:327